Monthly Notices
of the
ROYAL ASTRONOMICAL SOCIETY

MNRAS **433,** 1362–1368 (2013) doi:10.1093/mnras/stt804
Advance Access publication 2013 June 3

An X-ray–UV correlation in Cen X-4 during quiescence

E. M. Cackett,[1]⋆ E. F. Brown,[2] N. Degenaar,[3] J. M. Miller,[3] M. Reynolds[3] and R. Wijnands[4]

[1]*Department of Physics & Astronomy, Wayne State University, 666 W. Hancock St., Detroit, MI 48201, USA*
[2]*Department of Physics & Astronomy, National Superconducting Cyclotron Laboratory, and the Joint Institute for Nuclear Astrophysics, Michigan State University, East Lansing, MI 48824, USA*
[3]*Department of Astronomy, University of Michigan, 500 Church St, Ann Arbor, MI 48109-1042, USA*
[4]*Astronomical Institute 'Anton Pannekoek', University of Amsterdam, Science Park 904, NL-1098 XH Amsterdam, the Netherlands*

Accepted 2013 May 8. Received 2013 April 18; in original form 2012 October 16

ABSTRACT

Quiescent emission from the neutron star low-mass X-ray binary Cen X-4 is seen to be variable on time-scales from hundreds of seconds to years, suggesting that at least in this object, low-level accretion is important during quiescence. Here, we present results from recent *XMM–Newton* and *Swift* observations of Cen X-4, where the X-ray flux (0.5–10 keV) varies by a factor of 6.5 between the brightest and faintest states. We find a positive correlation between the X-ray flux and the simultaneous near-ultraviolet (UV) flux, where as there is no significant correlation between the X-ray and simultaneous optical (*V*, *B*) fluxes. This suggests that while the X-ray and UV emitting regions are somehow linked, the optical region originates elsewhere. Comparing the luminosities, it is plausible that the UV emission originates due to reprocessing of the X-ray flux by the accretion disc, with the hot inner region of the disc being a possible location for the UV emitting region. The optical emission, however, could be dominated by the donor star. The X-ray/UV correlation does not favour the accretion stream impact point as the source of the UV emission.

Key words: stars: neutron – X-rays: binaries – X-rays: individual: Cen X-4.

1 INTRODUCTION

Low-mass X-ray binaries (LMXBs) are often transient, cycling through periods of outburst and quiescence where the X-ray luminosity varies by over four orders of magnitude between the two. In quiescence, the accretion rate is at less than 10^{-4} of the Eddington limit. The transient behaviour of X-ray binaries (and dwarf novae) is broadly described by the disc instability model (see Lasota 2001, 2008 for a review) where a thermal–viscous instability causes an outburst. During an outburst accretion likely occurs via an optically thick, geometrically thin disc (e.g. Shakura & Sunyaev 1973). During quiescence, the picture is not quite as clear, and accretion is thought to occur in a very different manner. In order to describe both the long recurrence times for transients and the observed quiescent X-ray emission a standard thin disc must be truncated at large radii (e.g. Lasota 1996; Dubus, Hameury & Lasota 2001). Moreover, as the accretion rate drops, it is expected that the inner disc evaporates, leaving a hole (Meyer & Meyer-Hofmeister 1994).

Two component models for the quiescent accretion flow were therefore developed, where an outer truncated disc has an advection-dominated accretion flow (ADAF; Narayan & Yi 1994, 1995) inside (Narayan, McClintock & Yi 1996; Esin, McClintock & Narayan 1997; Narayan, Barret & McClintock 1997). Such models successfully explain the quiescent X-ray properties of black hole LMXBs, which are seen to display simple power-law emission. For neutron stars, there is the added complication of a stellar surface. The ADAF models predict that neutron stars should have a higher quiescent luminosity compared to black holes (with the same orbital period) as the hot flow can heat the neutron star surface, where as in black holes the energy will be advected through the event horizon (e.g., Garcia et al. 2001, and references therein). While such a difference is generally seen (though see Jonker et al. 2007 for a remarkable exception) it is also expected that quiescent neutron stars should be hot due to heating of the crust during the outburst ('deep crustal heating'; Brown, Bildsten & Rutledge 1998). Moreover, it is even possible that energy may go into a jet rather than being advected (Fender, Gallo & Jonker 2003).

The exact geometry and details of how the hot, radiatively inefficient accretion flows work during quiescence is still not clear. There is uncertainty as to whether the flow is an ADAF (Narayan & Yi 1994, 1995) or an advection-dominated flow with strong outflows (ADIOS; Blandford & Begelman 1999), and what the value of the standard viscosity parameter, α, is in quiescence (Menou et al. 2000;

⋆ E-mail: ecackett@wayne.edu

© 2013 The Authors
Published by Oxford University Press on behalf of the Royal Astronomical Society

Downloaded from http://mnras.oxfordjournals.org/ at Johns Hopkins University on November 6, 2013

Menou 2002). The truncation radius is usually assumed to be between 10^2 and 10^4 Schwarzschild radii (Esin et al. 1997), but it too is uncertain (Menou et al. 1999). How matter is accreted on to the neutron star is also not clear. The quiescent luminosities of neutron star LMXBs are low enough to require that much of the accreted matter is prevented from reaching the neutron star surface, which could happen via the propeller effect (Menou et al. 1999; Menou & McClintock 2001). Alternatively, the hot accretion flow may not be an ADAF (or ADIOS), but a hot settling flow instead (Medvedev & Narayan 2001; Narayan & Medvedev 2003). In this hot settling flow scenario, hot quasi-spherical accretion on to a spinning neutron star happens subsonically, and the flow essentially settles on to the rotating neutron star without a shock. The luminosity of this flow is then mostly generated as rotational energy is extracted from the neutron star, rather than from the mass accretion rate. Thus, there exists a range of models to explain how accretion happens during quiescence, and even the basic parameters of such models are not well constrained, at least in the case of neutron star LMXBs.

The mechanism behind accretion in quiescence therefore remains elusive. Yet, one signature that it must be occurring is sporadic X-ray variability. Such variability in quiescent emission from neutron stars has been seen in several objects on all time-scales studied – from hundreds of seconds to years (Campana et al. 1997, 2004; Rutledge et al. 2001, 2002; Cackett et al. 2005, 2010, 2011; Fridriksson et al. 2011). X-ray spectra of quiescent neutron stars typically show two components – both a thermal, blackbody-like component and a non-thermal power-law component. A recent study of long-term quiescent variability in Cen X-4 (Cackett et al. 2010) confirmed that the thermal component, as well as the power-law component, is variable. Interestingly, the power law and thermal fluxes appear to vary in tandem, contributing roughly the same fraction of the total flux at all epochs. This suggests a clear link between the two components during quiescence. Compton upscattering of soft photons from the neutron star surface in the hot accretion flow would seem to be an obvious link between these two components. However, it would produce a power law that is only a few per cent of the 0.5–10 keV flux (Menou & McClintock 2001), while we observe the components to be roughly equal (Cackett et al. 2010). The power law arising from shock emission between a radio pulsar wind and inflowing matter from the companion star (Campana & Stella 2003) also seems to be ruled out as the variability in Cen X-4 cannot be explained by correlated changes in column density and the power-law component (Cackett et al. 2010). The accretion flow getting all the way down to the neutron star surface may therefore be the most realistic mechanism for the synchronous change in both the neutron star surface temperature and the power-law component as the accretion rate varies (e.g. Stella et al. 1994; Menou & McClintock 2001).

In order to further investigate the nature of quiescent variability in neutron star LMXBs on time-scales of weeks to months we observed Cen X-4 with *XMM–Newton* four times between 2010 August and 2011 January. Importantly, we also obtain optical and ultraviolet (UV) photometry with *XMM–Newton* to investigate the nature of broad-band variability during quiescence. Combining these four new *XMM–Newton* observations with one archival *XMM–Newton* observation and two *Swift* observations we show a clear correlation between X-ray and UV flux during quiescence. Cen X-4 is one of very few objects where such an X-ray/UV study can be performed given its proximity and relatively low extinction. In Section 2, we describe the data reduction and analysis before describing our results in Section 3 and discussing their implications in Section 4.

2 DATA REDUCTION AND ANALYSIS

The four *XMM–Newton* observations were obtained between the end of 2010 August and 2011 January with each observation lasting between 10 and 20 ks. The ObsIDs are 0654470201, 0654470301, 0654470401, 0654470501 and their respective start dates (dd/mm/yy) are 25/08/10, 04/09/10, 24/01/11 and 31/01/11. The X-ray detectors were operated in full window mode with a medium filter. The Optical Monitor (OM; Mason et al. 2001) was operated such that data were collected in multiple optical/UV filters during the X-ray observations. In Table 1, we give details of all four observations along with exposure times for each instrument and filter used. The data were reduced with the *XMM–Newton* Science Analysis Software, version 11.0.0, using the latest calibration files.

In addition to the *XMM–Newton* data, we also analyse two *Swift* observations of Cen X-4 that also have both X-ray and optical/UV data. The ObsIDs 00035324001 and 00035324002 were performed on 03/09/06 and 01/05/12. The X-ray detector was operated in photon counting mode. In the first observation, only a *UVW*1 exposure was taken, where as in the second observation exposures in *V*, *B*, *U*, *UVW*1, *UVM*2 and *UVW*2 were taken. Table 2 gives details of the *Swift* observations. The data were reduced using HEASOFT, version 6.11.1. In the following sections, we detail the data reduction for the X-ray and optical/UV detectors.

2.1 X-ray data reduction

2.1.1 XMM–Newton

We created calibrated event files for each observation from the Observation Data Files using the emproc and epproc commands for the MOS and pn detectors. We check for periods of high background by

Table 1. Details of the new *XMM–Newton* observations of Cen X-4, including count rates and optical/UV fluxes. *AB* flux densities have units of erg s^{-1} cm^{-2} Å. ND indicates that the source was not detected in that filter. MOS and pn net count rates are given in the 0.5–10 keV energy range. The count rate is given for MOS 1 only, the MOS 2 rate is always very similar.

Detector	0654470201			0654470301			0654470401			0654470501		
or filter	Exp. (ks)	Net rate (10^{-1} c s^{-1})	*AB* flux (10^{-17})	Exp. (ks)	Net rate (10^{-1} c s^{-1})	*AB* flux (10^{-17})	Exp. (ks)	Net rate (10^{-1} c s^{-1})	*AB* flux (10^{-17})	Exp. (ks)	Net rate (10^{-1} c s^{-1})	*AB* flux (10^{-17})
MOS	11.2	0.75 ± 0.03	–	19.3	0.84 ± 0.02	–	14.4	1.20 ± 0.03	–	13.4	0.39 ± 0.02	–
pn	10.4	3.07 ± 0.07	–	16.1	3.73 ± 0.05	–	11.3	4.21 ± 0.06	–	10.5	1.59 ± 0.04	–
V	4.0	6.2 ± 0.6	15.5 ± 1.4	2.86	9.2 ± 0.7	23.1 ± 1.8	1.76	5.1 ± 0.8	12.8 ± 2.1	1.76	4.8 ± 0.8	12.0 ± 2.0
B	3.0	7.0 ± 0.8	8.7 ± 1.0	0.0	–	–	1.76	8.2 ± 1.0	10.2 ± 1.2	1.76	6.4 ± 1.0	8.0 ± 1.2
U	1.98	2.9 ± 0.6	5.6 ± 1.2	3.76	4.6 ± 0.5	8.8 ± 0.9	1.76	5.0 ± 0.6	9.7 ± 1.2	1.76	2.6 ± 0.6	5.0 ± 1.2
*UVW*1	5.0	1.7 ± 0.2	8.3 ± 1.1	3.76	1.8 ± 0.3	8.8 ± 1.3	1.76	2.4 ± 0.4	11.5 ± 2.0	1.76	0.42 ± 0.36	2.0 ± 1.7
*UVM*2	5.0	0.37 ± 0.14	8.2 ± 3.0	5.0	ND	ND	4.2	0.57 ± 0.15	12.6 ± 3.3	3.2	ND	ND

Table 2. Details of the *Swift* observations of Cen X-4, including count rates and optical/UV fluxes. *AB* flux densities have units of erg s^{-1} cm^{-2} Å. X-ray Telescope (XRT) net count rates are given in the 0.5–10 keV energy range.

Detector	00035324001			00035324002		
or filter	Exp. (ks)	Net rate (10^{-1} c s^{-1})	*AB* flux (10^{-17})	Exp. (ks)	Net rate (10^{-1} c s^{-1})	*AB* flux (10^{-17})
XRT	4.5	0.38 ± 0.03	–	3.8	0.76 ± 0.05	–
V	–	–	–	0.30	0.75 ± 0.07	19.5 ± 2.0
B	–	–	–	0.30	1.11 ± 0.10	16.5 ± 1.4
U	–	–	–	0.30	1.35 ± 0.09	22.5 ± 1.5
*UVW*1	6.25	0.32 ± 0.01	15.0 ± 0.5	0.61	0.55 ± 0.04	25.6 ± 1.9
*UVM*2	–	–	–	0.95	0.29 ± 0.02	24.4 ± 1.8

creating light curves from the entire detectors with 100 s time binning, filtering for events with energies >10 keV and PATTERN = 0 for the MOS, and $10 < E < 12$ keV and PATTERN = 0 for the pn.

The background was high throughout the entire first observation (0654470201), with the MOS 1 count rate ranging from 0.2–3.7 c s^{-1}, and the pn count rate from 2.6–15.2 c s^{-1}. Filtering out the periods of particularly high background would leave only a very small exposure left; thus, we include all the available data. The other three observations had some short periods of background flaring at either the beginning or end of the observations, but the background was mostly low throughout. The periods of background flaring were never as bad as the first observation, and therefore we include all available data. Only in the first observation does the significant flaring there notably reduce the signal-to-noise ratio.

For both the MOS and pn detectors, we extract the source spectrum from a circular region of radius 20 arcsec, and the background spectrum from a nearby, source-free 2 arcmin region. The response files are generated with the arfgen and rmfgen tools, and the resulting spectrum is binned to a minimum of 25 counts per bin. We give net count rates in Table 1.

2.1.2 *Swift*

Calibrated event files were created by reprocessing the data using the XRTPIPELINE tool and applying the standard (default) screening criteria. We analyse data taken in photon counting mode. We extracted the source spectrum using XSELECT, and a circular extraction region with a 20 pixel radius. The background spectrum was extracted from an annulus with inner radius of 40 pixels and outer radius of 120 pixels. We use the XRTMKARF tool to create the ancillary response file, and use the appropriate response matrix based on the epoch of the observation and the observing mode. Given the shorter exposures and lower count rates compared to *XMM–Newton* we only bin spectra to 10 counts per bin.

2.2 Optical/UV data

2.2.1 *XMM–Newton*

We observed Cen X-4 with the OM in imaging mode. However, rather than using the standard set-up, we chose to more efficiently obtain exposures of Cen X-4 in five filters by using a Science User Defined mode whereby only a single window is used to observe just the centre of the field of view (normally a mosaic is created from multiple windows to cover a much larger field of view). In this way, we were able to obtain images in the following filters during the short X-ray exposures of Cen X-4 (effective wavelengths are given): *V* (5407 Å), *B* (4334 Å), *U* (3472 Å), *UVW*1 (2905 Å) and *UVM*2 (2298 Å).

Table 3. *XMM–Newton* obsID 0144900101, optical/UV details. *AB* flux densities have units of erg s^{-1} cm^{-2} Å.

Filter	Exp. (ks)	Net rate (10^{-1} c s^{-1})	*AB* flux (10^{-17})
V	4.0	8.3 ± 0.5	20.8 ± 1.2
B	4.0	13.9 ± 0.5	17.3 ± 0.7
U	4.0	6.6 ± 0.3	12.7 ± 0.7
*UVW*1	12.2	3.7 ± 0.1	18.0 ± 0.5
*UVM*2	19.8	0.81 ± 0.05	17.9 ± 1.0
*UVW*2	25.0	0.25 ± 0.07	14.5 ± 3.8

We reduce the OM data using the OMICHAIN tool. This tool processes the data with the latest calibration files, and then performs source detection and aperture photometry. The output files include both the images for each filter along with a combined source list containing detailed parameters for each source detected in all exposures, including the count rate (corrected for instrumental effects such as detector dead time) and *AB* flux densities (in erg s^{-1} m^{-2} $Å^{-1}$). We visually identified Cen X-4 in all images before finding the corresponding source in the source list. In observation 0654470301 Cen X-4 was not automatically detected in the *UVM*2 filter, though a faint excess in counts did seem apparent on visual inspection. We therefore ran the OMDETECT tool (part of the OMICHAIN pipeline) on its own with the significance reduced to only requiring 1σ above the background; however, the source was still not detected (note the default is a 3σ threshold). Similarly, in observation 0654470501 the source was not automatically detected in *UVW*1 or *UVM*2. Once again, it did seem present (though faint) on manual inspection of the image, and we therefore re-ran the OMDETECT tool with only a 1σ threshold. This led to a detection of Cen X-4 in *UVW*1 with only a 1.9σ significance, while there was still no positive detection in the *UVM*2 filter. Count rates and *AB* flux densities are given for each observation in Table 1. There is clearly variability seen between the different observations.

We also note that only one of the two archival *XMM–Newton* observations (ObsID:0144900101) also has OM data. This observation took place starting on 2003 March 1, with exposures in *V*, *U*, *B*, *UVW*1, *UVM*2 and *UVW*2 filters. The data were taken in imaging mode, using the default setup whereby a series of five exposures are taken in each filter, and then combined together in a mosaic to fill the 17 arcmin field of view. During each exposure, the central 2 arcmin region is always observed. We reduced the data in the same manner, using the OMICHAIN tool once again. The exposure times, corrected count rates and fluxes for each filter are given in Table 3.

2.2.2 *Swift*

The two *Swift* observations also include optical/UV observations using the Ultra-Violet/Optical Telescope (UVOT; Roming et al. 2005; Breeveld et al. 2010). The filters are similar, though slightly different, to the *XMM–Newton* filters. The first observation used the *UVW*1 filter exclusively, where as the second observation used *V* (5468 Å), *B* (4392 Å), *U* (3465 Å), *UVW*1 (2600 Å), *UVM*2 (2246 Å) and *UVW*2 (1928 Å) filters (wavelengths from Poole et al. 2008). Note that both the *UVW*1 and *UVW*2 filters are broader than the *UVM*2 filter, and hence are more sensitive. However, *UVW*1 and *UVW*2 also have red leaks, meaning that their sensitivity stretches to

Table 4. Spectral fit parameters. The flux is given in units of erg s^{-1} cm^{-2}. The column density was fixed at $N_H = 4.9 \times 10^{20}$ cm^{-2} in all spectral fits. We also assumed a neutron star radius of 10 km and mass of 1.4 $M_\odot$, and a distance to Cen X-4 of 1.2 kpc. The power-law normalization is defined as photons keV^{-1} cm^{-2} s^{-1} at 1 keV. We define that the thermal fraction is the ratio of the unabsorbed 0.5–10 keV thermal flux to the total unabsorbed 0.5–10 keV flux.

	XMM–Newton				*Swift*	
Parameter	0654470201	0654470301	0654470401	0654470501	00035324001	00035324002
$kT_{\rm eff}^{\infty}$ (eV)	55.9 ± 0.7	56.5 ± 0.3	60.8 ± 0.3	49.0 ± 0.6	62.4 ± 2.3	65.2 ± 5.7
Power-law index, Γ	1.77 ± 0.21	1.62 ± 0.10	1.38 ± 0.10	1.94 ± 0.19	1.51 ± 0.86	1.79 ± 0.53
Power-law norm (10^{-5})	6.6 ± 1.4	6.3 ± 0.7	5.5 ± 0.7	3.6 ± 0.7	$5.8^{+7.5}_{-4.8}$	$29.1^{+22.4}_{-13.5}$
Unabs. 0.5–10 keV flux (10^{-12})	0.92 ± 0.08	1.00 ± 0.02	1.31 ± 0.03	0.44 ± 0.01	1.38 ± 0.38	2.85 ± 0.30
Thermal fraction (per cent)	58	56	62	59	68	41
χ^2_ν (dof)	0.91 (106)	0.93 (168)	0.99 (129)	1.27 (71)	1.31 (13)	0.67 (24)

longer (redder) wavelengths than *UVM*2. We used the UVOTMAGHIST tool to perform aperture photometry, using a 3 arcsec radius circular extraction region, and a circular, source-free nearby background region with a 12 arcsec radius. This tool performs photometry on all separate exposures for a given filter, applies the aperture correction and determines the *AB* flux. Having determined the count rates and fluxes for each individual exposure, we calculate the exposure-weighted average count rate and flux, as given in Table 2.

2.3 X-ray spectral analysis

We fit the X-ray spectra using XSPEC version 12.7.0 (Arnaud 1996). Each observation is fitted separately, but when fitting the individual *XMM–Newton* observations we jointly fit the MOS 1, MOS 2 and pn spectra, with the parameters being the same for all detectors. We fit the spectra using a neutron star atmosphere plus a power law, all modified by Galactic photoelectric absorption. We use the nsatmos model for the neutron star atmosphere (Heinke et al. 2006). This is the same model we used to fit six previous observations of Cen X-4 (Cackett et al. 2010), thus, allowing for a direct comparison with these previous results.[1] For the same reason, we choose to fix $N_H = 4.9 \times 10^{20}$ cm^{-2}, the value we found from jointly fitting six previous observations in Cackett et al. (2010). Also, to allow a direct comparison with our previous results, we fix the distance to 1.2 kpc (Chevalier et al. 1989) in the spectral fits. In Cackett et al. (2010), we investigated which parameters were variable, finding that the thermal component and the power-law component both must vary. For the thermal component, either the effective temperature, emitting radius or both can vary, and we found that equally good fits are achieved regardless of which parameter is left variable. Here, for simplicity, we fix the neutron star radius and allow the temperature to vary between epochs. This choice does not affect the results since the thermal component can be fitted equally well with either a variable temperature or a variable radius, and it is only the flux that we are mostly concerned with here. We assume a neutron star with $R = 10$ km and $M = 1.4\,M_\odot$, and that the entire surface is emitting. We fit the spectra in the 0.5–10 keV range and best-fitting parameters are given in Table 4. Uncertainties are quoted at the 1σ level throughout.

3 RESULTS

The long-term X-ray quiescent light curve of Cen X-4 is shown in Fig. 1, where we include the observations from Cackett et al. (2010) as well as the four new *XMM–Newton* and two *Swift* observations presented here. Notably, significant variability is seen on the weeks to months time-scales probed by these new observations. Most significant is the factor of 3 drop in flux between the third and fourth observations taken at the end of 2011 January and separated by only 7 d.

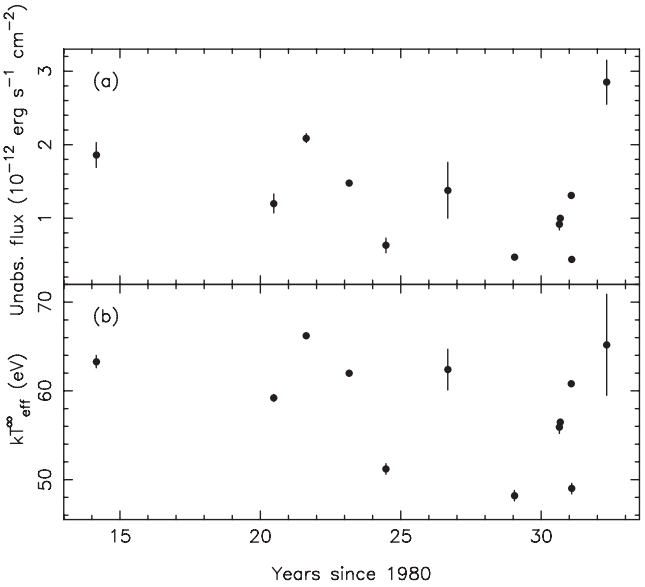

Figure 1. Long-term X-ray quiescent light curve of Cen X-4, showing variability on all time-scales. (a) Unabsorbed 0.5–10 keV flux, (b) Effective temperature for an observer at infinity.

It is clear from looking at the OM count rates and fluxes (Table 1) that Cen X-4 is also highly variable in the optical/UV part of the spectrum during quiescence. In Fig. 2, we plot the optical/UV fluxes against the 0.5–10 keV unabsorbed X-ray flux. In order to compare the energetics, we convert the flux densities (erg s^{-1} m^{-2} $Å^{-1}$) that are the output from the OMICHAIN to fluxes by multiplying by the full width at half-maximum of the filter bandpass. We use: 684 Å (*V*), 976 Å (*B*), 810 Å (*U*), 620 Å (*UVW*1), 439 Å (*UVM*2) for the *XMM–Newton* filters, and 769 Å (*V*), 975 Å (*B*), 785 Å (*U*), 693 Å (*UVW*1), 498 Å (*UVM*2) for the *Swift* filters. We also de-redden the UV/optical fluxes. We use the gas-to-dust ratio from Güver & Özel (2009) in order to convert from equivalent hydrogen column to $E(B-V)$. We then use the interstellar extinction curve of Cardelli, Clayton & Mathis (1989) to estimate the extinction correction at the wavelengths of each filter.

We test for a correlation between the optical/UV and X-ray fluxes using a simple Pearson's linear correlation test. The correlation

[1] This previous analysis looked at data from a range of different missions (1 *ASCA*, 2 *Chandra*, 2 *XMM* and 1 *Suzaku*).

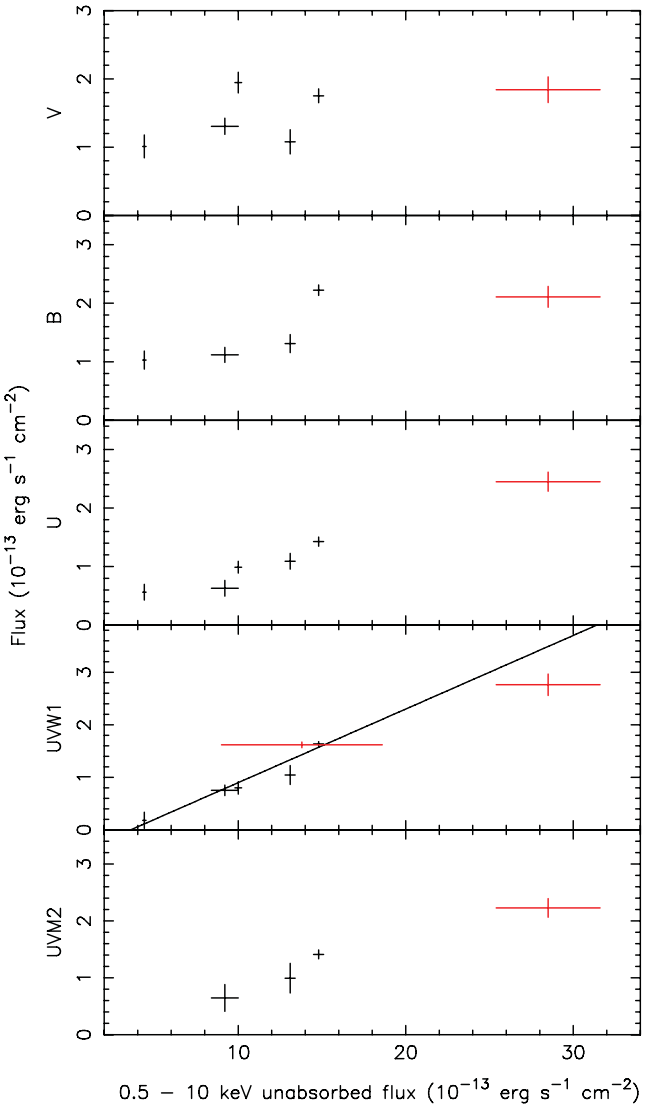

Figure 2. De-reddened optical and UV fluxes versus 0.5–10 keV unabsorbed flux from *XMM–Newton* (black) and *Swift* (red). A clear correlation between the X-ray and the *U*, *UVW*1 and *UVM*2 fluxes is apparent. The solid line shows the best-fitting straight line to the *UVW*1/X-ray points, with equation $f_{\rm UV} = (0.14 \pm 0.01) f_{\rm X} - (0.50 \pm 0.18)$.

coefficients we find are $r = 0.554$, 0.779, 0.982, 0.973, 0.976 for the *V*, *B*, *U*, *UVW*1 and *UVM*2 filters, respectively. Given the number of data points, and a two-tail test (no a priori knowledge of positive or negative correlation), this corresponds to a positive correlation at the 0.746, 0.880, 0.999 52, 0.999 77 and 0.976 confidence levels. Thus, the *U* and *UVW*1 fluxes are correlated with the X-ray flux at greater than 3σ, while the *UVM*2 flux is correlated at greater than 2σ. There is no significant correlation between the *V* or *B* fluxes and the X-ray flux, indicating that this is a UV only correlation. We also look to see if there is a correlation between *UVW*1 and *V* band fluxes, finding $r = 0.63$, which corresponds to a positive correlation at the 0.816 confidence level. Thus, there is no significant correlation between the *V* band and *UVW*1 fluxes.

We now concentrate on the *UVW*1 versus X-ray correlation further, given that it is the most significant correlation. Obviously, given the high linear correlation coefficient, a simple straight line fits the *UVW*1 – X-ray correlation well. We get the following best-fitting parameters: $f_{\rm UV} = (0.14 \pm 0.01) f_{\rm X} - (0.50 \pm 0.18)$, giving a reduced $\chi^2 = 1.35$. We also test fitting a power law of the form $f_{\rm UV} = a(f_{\rm X} - f_{\rm X0})^b$, where $f_{\rm X0}$ is a constant to allow a non-zero X-ray flux when $f_{\rm UV} = 0.0$, or vice versa. The best fit is very close to a linear relationship, with $b = 1.00^{+0.34}_{-0.14}$, and giving a reduced $\chi^2 = 1.69$. If we fit a power law with the index, *b* fixed at 0.5 (as expected for reprocessing by van Paradijs & McClintock 1994), we get a worse fit (reduced $\chi^2 = 4.5$). However, with only seven data points we can clearly not make any strong conclusions about the form of the correlation, especially as there is only one observation at a high luminosity, where a deviation from a linear relationship would become apparent. We also caution that we are comparing *UVW*1 fluxes with both *Swift* and *XMM–Newton* – the filter responses and wavelength range are slightly different between the missions which could lead to a small offset between the two. Further data are needed to strengthen and define the shape of the correlation.

We also look for whether there is an X-ray/UV correlation on shorter time-scales by looking at the UV and X-ray light curve during the two *Swift* observations. This is possible with *Swift* because the observations consist of multiple ∼1 ks exposures, each giving separate UV images. With *XMM–Newton*, however, there is only one exposure in each filter during the entire observation and so we cannot look for X-ray–UV correlations during the *XMM–Newton* observations. The first *Swift* observation consists of six *Swift* orbits of data, and the *UVW*1 filter was used for all of them. We can therefore compare the X-ray and UV light curves on time-scales of a few thousand seconds. The second *Swift* observation comprised three orbits, with a *UVW*1 exposure during each orbit. For both observations, we create a background-subtracted *Swift*/X-ray Telescope (XRT) light curves, using the XRTLCCORR tool to perform count rates corrections for vignetting, point spread function, etc. The *UVW*1 count rates are determined using the UVOTMAGHIST tool (as described above). We show the light curves in Fig. 3. The XRT and *UVW*1 count rates are generally well correlated during both observations.

The *XMM–Newton* observations only perform one exposure in each filter during a given observation. Therefore, while the X-ray flux we obtain is from the entire observation, the optical/UV fluxes are only obtained during some fraction of the observation. The X-ray exposures range from approximately 10–20 ks, where as the optical/UV exposures are between 1.76 and 5 ks. Variability during the observation could therefore add scatter to the UV and X-ray correlations. Examining the X-ray light curves from the *XMM–Newton* observations there is variability present (as has also been seen during previous *XMM–Newton* and *Chandra* observations; see, e.g., Campana et al. 2004; Cackett et al. 2010). However, any subset of 2 ks or longer will not deviate too far from the mean X-ray flux, and thus not add a large amount of scatter.

4 DISCUSSION AND CONCLUSIONS

Our observations of Cen X-4 during quiescence have shown that the X-ray and near-UV emission are correlated, where as there is no significant correlation between the X-ray and optical emission. The X-ray/UV correlation is seen both on time-scales of weeks–years, as well as during observations spanning less than one day. In order to investigate the physical origin of this correlation, it is important to consider the energetics – if the correlation is due to reprocessing of the X-ray emission, then the near-UV flux must be only a fraction of the X-ray flux.

We find that the *UVW*1 flux is approximately 10 per cent of the 0.5–10 keV flux. However, much of the X-ray flux from the hot

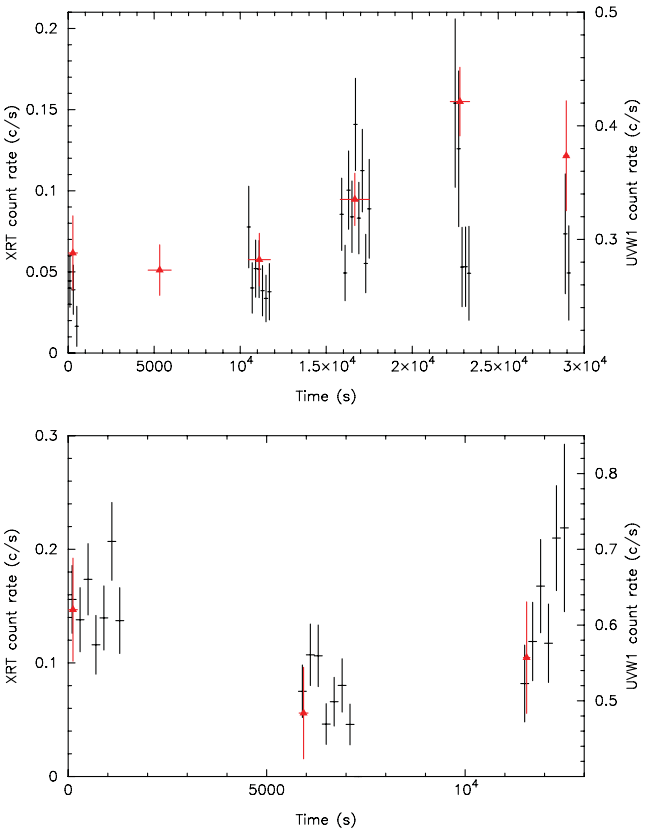

Figure 3. *Swift* X-ray (black) and *UVW*1 (red, triangles) light curves during the first (top) and second (bottom) *Swift* observations (00035324001 and 00035324002). The XRT data have 200 s time binning.

neutron star surface is emitted below 0.5 keV, and thus it is important to take this flux into consideration. Furthermore, the power-law component will likely extend beyond 10 keV, though its shape there is uncertain. To provide an estimate for the total X-ray flux, we extrapolate the best-fitting neutron star atmosphere plus power-law models to cover the range 0.01–100 keV. For the faintest observation (*XMM–Newton*: 0654470501) we find a factor of 3 increase in the flux, where as for the brightest observation (*Swift*: 00035324002) we find a factor of 2.6 increase. The higher temperature during the brighter observation means more of the neutron star atmosphere flux is in the 0.5–10 keV band; hence, the slightly lower increase in flux when extending the energy range. Of course, the near-UV emission is in more than just the *UVW*1 filter. Combining the *U*, *UVW*1 and *UVM*2 fluxes, we get an increase by a factor of 4.0 and 2.7 for the faintest and brightest observations, respectively, over using just the *UVW*1 flux. Thus, when accounting for emission over a wider wavelength range, the near-UV flux is still approximately 10 per cent of the X-ray flux. Such a fraction of the X-ray flux is reasonable for reprocessed emission.

van Paradijs & McClintock (1994) consider X-ray reprocessing in the accretion disc and show that the reprocessed emission should be proportional to $L_{\rm X}^{1/2}R$, where R is the outer radius of the accretion disc. We, however, find that the UV flux increases approximately linearly with the X-ray flux and a power law with index of 0.5 does give a significantly worse fit. However, with the limited number of observations and range in flux the exact relationship is uncertain, and would be significantly strengthened by further data. Considering the relevant time-scales for reprocessing, the light travel time from the neutron star to the outer disc is less than 1 s, and so we would not expect to see any time delay between the X-ray and UV light curves. This is what we observe (Fig. 3) where the X-ray and UV vary in tandem during *Swift* observations. The viscous time-scale from the outer disc in these objects is significantly longer (of the order of weeks), and therefore cannot be used to explain the simultaneous variability in UV and X-rays.

Another source where a similar correlation has been found is the quiescent black hole V404 Cyg, where a correlation between X-ray and Hα emission has been previously observed (Hynes et al. 2004), with a weaker correlation between the X-ray flux and the optical continuum. Irradiation/reprocessing can readily explain that correlation as the entire Hα line is seen to respond quickly to X-ray variability. Here too, we see that the X-ray and UV flux seem to respond simultaneously during the *Swift* observations (see Fig. 3), though we do not have the data to be able to establish any lag. This prompt response also supports irradiation/reprocessing as the origin of the correlation observed here. However, we do not observe any clear correlation between the optical continuum and the X-ray flux (unlike in V404 Cyg), which would suggest that the UV and optical emitting regions are well separated. Alternatively, it could just be the case that in Cen X-4, the optical flux is dominated by the donor star, and so any change in optical flux due to reprocessing may be too small to see. Furthermore, the longer orbital period of V404 Cyg (6.5 d compared to 15 h for Cen X-4; Cowley et al. 1988; Casares, Charles & Naylor 1992) will lead to a larger disc, which would be more luminous at optical wavelengths.

The optical emission could be dominated by the donor star, as well as some contribution from the cooler outer regions of the truncated accretion disc. The UV emission is too hot to arise from the donor star, and the X-ray/UV correlation suggests it must arise from a region that can see the central X-ray source, such as the inner region of the truncated accretion disc. The correlation between X-ray and UV flux would seem to rule out the accretion stream impact point as the location for the UV emission, which had been previously suggested by McClintock & Remillard (2000) based on the Mg II λ2800 emission line in an *Hubble Space Telescope*/STIS spectrum of Cen X-4 not showing a double-peak as would be expected for emission from the disc. Hynes & Robinson (2012) closely examine the UV Spectral Energy Distributions (SEDs) of three quiescent black hole and one quiescent neutron star and also rule out the stream impact point as the origin of the UV emission. They find that the mass accretion rate required to give the observed UV emission at the stream impact point in the black hole GU Mus and neutron star Aql X-1 is 10 times higher than realistic average rates from these source based on their accretion histories. They therefore favour an origin for the UV emission as being located in the hot inner region of the disc as also suggested by Campana & Stella (2000) and McClintock et al. (2003). Our results also support such a picture.

It is important to consider whether there is a viable alternative to X-ray reprocessing as the origin of the X-ray/UV correlation. For instance, could the emission in Cen X-4 be jet dominated and hence the UV flux and X-ray power law both originate from the jet? While radio emission has never been detected from a quiescent neutron star, it has been detected in quiescence in black hole X-ray binaries. For instance, a radio detection of the black hole A0620−00 in quiescence (Gallo et al. 2006) implies that there is a radio-emitting outflow during quiescence. Broad-band modelling of the quiescent SED in A0620−00 shows that the emission can be fitted with a maximally jet-dominated model with the jet emission dominating from radio through to the soft X-rays (Gallo et al. 2007) and implies that there are strong outflows (Froning et al. 2011). Similarly, V404 Cyg has been detected at radio wavelengths in quiescence

(Hjellming et al. 2000; Gallo, Fender & Hynes 2005; Hynes et al. 2009), with the radio spectrum consistent with synchrotron emission from a steady jet (Gallo et al. 2005). In fact, it has been shown that quiescent black hole X-ray binaries could all be in jet-dominated states (Fender et al. 2003). Neutron stars X-ray binaries, on the other hand, are known to be a factor of 30 or so fainter radio sources than black hole binaries during outburst (Fender & Kuulkers 2001; Migliari et al. 2003), and thus, if they follow the same dependence between the X-ray luminosity, L_X, and radio luminosity, L_R, then neutron stars could also be jet dominated although at lower Eddington fractions (Fender et al. 2003). However, neutron stars have been shown to have a different dependence between L_X and L_R, implying that they never reach a jet-dominated state and remain X-ray dominated (Migliari & Fender 2006). This therefore suggests that jet emission is unlikely to account for the X-ray/UV correlation observed here in Cen X-4.

In conclusion, we have observed a significant X-ray/UV correlation in Cen X-4, whose most likely explanation is due to irradiation of the inner edge of a truncated accretion disc by a central X-ray source leading to reprocessed UV emission. Further X-ray/UV monitoring will help more firmly establish the link between X-ray and UV emission in Cen X-4.

ACKNOWLEDGEMENTS

EMC thanks Rob Hynes, Edward Robinson and Federico Bernardini for helpful discussions on UV emission during quiescence. RW acknowledges support from a European Research Council (ERC) starting grant. ND is supported by NASA through Hubble postdoctoral fellowship grant number HSTHF-51287.01-A from the Space Telescope Science Institute. We acknowledge the use of public data from the Swift data archive.

REFERENCES

Arnaud K. A., 1996, in Jacoby G. H., Barnes J., eds, ASP Conf. Ser. Vol. 101, XSPEC: The First Ten Years. Astron. Soc. Pac., San Francisco, p. 17
Blandford R. D., Begelman M. C., 1999, MNRAS, 303, L1
Breeveld A. A. et al., 2010, MNRAS, 406, 1687
Brown E. F., Bildsten L., Rutledge R. E., 1998, ApJ, 504, L95
Cackett E. M. et al., 2005, ApJ, 620, 922
Cackett E. M., Brown E. F., Miller J. M., Wijnands R., 2010, ApJ, 720, 1325
Cackett E. M., Fridriksson J. K., Homan J., Miller J. M., Wijnands R., 2011, MNRAS, 414, 3006
Campana S., Stella L., 2000, ApJ, 541, 849
Campana S., Stella L., 2003, ApJ, 597, 474
Campana S., Mereghetti S., Stella L., Colpi M., 1997, A&A, 324, 941
Campana S., Israel G. L., Stella L., Gastaldello F., Mereghetti S., 2004, ApJ, 601, 474
Cardelli J. A., Clayton G. C., Mathis J. S., 1989, ApJ, 345, 245
Casares J., Charles P. A., Naylor T., 1992, Nat, 355, 614
Chevalier C., Ilovaisky S. A., van Paradijs J., Pedersen H., van der Klis M., 1989, A&A, 210, 114
Cowley A. P., Hutchings J. B., Schmidtke P. C., Hartwick F. D. A., Crampton D., Thompson I. B., 1988, AJ, 95, 1231
Dubus G., Hameury J.-M., Lasota J.-P., 2001, A&A, 373, 251
Esin A. A., McClintock J. E., Narayan R., 1997, ApJ, 489, 865
Fender R. P., Kuulkers E., 2001, MNRAS, 324, 923
Fender R. P., Gallo E., Jonker P. G., 2003, MNRAS, 343, L99
Fridriksson J. K. et al., 2011, ApJ, 736, 162
Froning C. S. et al., 2011, ApJ, 743, 26
Gallo E., Fender R. P., Hynes R. I., 2005, MNRAS, 356, 1017
Gallo E., Fender R. P., Miller-Jones J. C. A., Merloni A., Jonker P. G., Heinz S., Maccarone T. J., van der Klis M., 2006, MNRAS, 370, 1351
Gallo E., Migliari S., Markoff S., Tomsick J. A., Bailyn C. D., Berta S., Fender R., Miller-Jones J. C. A., 2007, ApJ, 670, 600
Garcia M. R., McClintock J. E., Narayan R., Callanan P., Barret D., Murray S. S., 2001, ApJ, 553, L47
Güver T., Özel F., 2009, MNRAS, 400, 2050
Heinke C. O., Rybicki G. B., Narayan R., Grindlay J. E., 2006, ApJ, 644, 1090
Hjellming R. M., Rupen M. P., Mioduszewski A. J., Narayan R., 2000, Astron. Telegram, 54, 1
Hynes R. I., Robinson E. L., 2012, ApJ, 749, 3
Hynes R. I. et al., 2004, ApJ, 611, L125
Hynes R. I., Bradley C. K., Rupen M., Gallo E., Fender R. P., Casares J., Zurita C., 2009, MNRAS, 399, 2239
Jonker P. G., Steeghs D., Chakrabarty D., Juett A. M., 2007, ApJ, 665, L147
Lasota J. P., 1996, in van Paradijs J., van den Heuvel E. P. J., Kuulkers E., eds, Proc. IAU Symp. 165, Compact Stars in Binaries. Kluwer, Dordrecht, p. 43
Lasota J.-P., 2001, New Astron. Rev., 45, 449
Lasota J.-P., 2008, New Astron. Rev., 51, 752
Mason K. O. et al., 2001, A&A, 365, L36
McClintock J. E., Remillard R. A., 2000, ApJ, 531, 956
McClintock J. E., Narayan R., Garcia M. R., Orosz J. A., Remillard R. A., Murray S. S., 2003, ApJ, 593, 435
Medvedev M. V., Narayan R., 2001, ApJ, 554, 1255
Menou K., 2002, in Gänsicke B. T., Beuermann K., Reinsch K., eds, ASP Conf. Ser. Vol. 261, The Quiescence of Dwarf Novae and X-ray Transients. Astron. Soc. Pac., San Francisco, p. 387
Menou K., McClintock J. E., 2001, ApJ, 557, 304
Menou K., Esin A. A., Narayan R., Garcia M. R., Lasota J.-P., McClintock J. E., 1999, ApJ, 520, 276
Menou K., Hameury J.-M., Lasota J.-P., Narayan R., 2000, MNRAS, 314, 498
Meyer F., Meyer-Hofmeister E., 1994, A&A, 288, 175
Migliari S., Fender R. P., 2006, MNRAS, 366, 79
Migliari S., Fender R. P., Rupen M., Jonker P. G., Klein-Wolt M., Hjellming R. M., van der Klis M., 2003, MNRAS, 342, L67
Narayan R., Medvedev M. V., 2003, MNRAS, 343, 1007
Narayan R., Yi I., 1994, ApJ, 428, L13
Narayan R., Yi I., 1995, ApJ, 452, 710
Narayan R., McClintock J. E., Yi I., 1996, ApJ, 457, 821
Narayan R., Barret D., McClintock J. E., 1997, ApJ, 482, 448
Poole T. S. et al., 2008, MNRAS, 383, 627
Roming P. W. A. et al., 2005, Space Sci. Rev., 120, 95
Rutledge R. E., Bildsten L., Brown E. F., Pavlov G. G., Zavlin V. E., 2001, ApJ, 551, 921
Rutledge R. E., Bildsten L., Brown E. F., Pavlov G. G., Zavlin V. E., 2002, ApJ, 577, 346
Shakura N. I., Sunyaev R. A., 1973, A&A, 24, 337
Stella L., Campana S., Colpi M., Mereghetti S., Tavani M., 1994, ApJ, 423, L47
van Paradijs J., McClintock J. E., 1994, A&A, 290, 133

This paper has been typeset from a TEX/LATEX file prepared by the author.